Peer-reviewed version available at C 2018, 4, 7; doi:10.3390/c4010007

Review

Hybrid Carbon-based Clathrates for Energy Storage

Kwai S. Chan*

Southwest Research Institute, San Antonio, Texas, USA; kchan@swri.org
* Correspondence: kchan@swri.org; Tel.: +1-210-522-2053

Abstract: Hybrid carbon-silicon, carbon-nitrogen, and carbon-boron clathrates are new classes of Type I carbon-based clathrates that have been identified by first-principles computational methods by substituting atoms on the carbon clathrate framework with Si, N, and/or B atoms. The hybrid framework is further stabilized by embedding appropriate guest atoms within the cavities of the cage structure. Series of hybrid carbon-silicon, carbon-boron, carbon-nitrogen, and carbon-silicon-nitrogen clathrates have been shown to exhibit small positive values of the energy of formation, indicating that they may be metastable compounds and amenable to fabrication. In this overview article, the energy of formation, elastic properties, and electronic properties of selected hybrid carbon-based clathrates are summarized. Theoretical calculations that explore the potential applications of hybrid carbon-based clathrates as energy storage materials, electronic materials, or hard materials are presented. The computational results identify compositions of hybrid carbon-silicon and carbon-nitrogen clathrates that may be considered candidate materials for use as either electrode materials for Li-ion batteries or as hydrogen storage materials. Prior processing routes for fabricating selected hybrid carbon-based clathrates are highlighted and difficulties encountered are discussed.

Keywords: carbon clathrates; hybrid carbon-silicon clathrates; hybrid carbon-nitrogen clathrates; electrode materials; hydrogen storage materials; energy storage materials; hard materials

1. Introduction

Type I and Type II carbon clathrates (C_{46} and C_{136}), which can be considered as analogs of carbon fullerene materials, are composed with face-sharing C_{20}, C_{24}, and C_{28} cages linked through sp^3-covalent bonds. Theoretical computations have shown that both Type I carbon clathrate (C_{46}) and Type II carbon clathrate (C_{136}) may exist as metastable phases under high pressures [1-3]. The cage structure of Type I carbon clathrate, C_{46}, is shown in Figure 1. Insertion of guest atoms such as Li, Na, or Ba into the cage structures has been predicted to be feasible under high pressures. However, the energies of formation for the Type I and Type II carbon clathrates are extremely high and neither Type I nor Type II carbon clathrates have been synthesized. On the other hand, Type I and Type II silicon clathrates (Si_{46} and Si_{136}), which are composed with face-sharing Si_{20}, Si_{24}, and Si_{28} cages, have been synthesized via a number of processing routes. Furthermore, various types of Type I and Type II silicon-based clathrates have also been synthesized with and without framework substitution. Substitution of the framework Si atoms with alloying elements such as Al, Cu, Ni, Ag, and among others, Zn have been reported [4]. The framework substituted compounds are actually more stable and exhibit improved electronic, thermoelectrical, and superconductive properties compared to the stoichiometric counterparts. These experimental observations suggest that it might be possible to develop a new class of hybrid carbon clathrates by substituting the carbon framework in C_{46} or C_{136} with Si, nitrogen or boron atoms.

The aim of this article is to review the current research on hybrid carbon-based clathrates, including the theoretical basis of the compounds and their properties, the synthesis of selected compounds, and their potential applications as energy storage materials. The current status of carbon clathrates is summarized first. The applications of first-principles methods to designing and

Preprints (www.preprints.org) | NOT PEER-REVIEWED | Posted: 18 January 2018 doi:10.20944/preprints201801.0166.v1

Peer-reviewed version available at C 2018, 4, 7; doi:10.3390/c4010007

identifying potential hybrid carbon-silicon clathrates are then highlighted. The potential applications of these hybrid carbon clathrates as energy storage materials, electronic or electrode materials, as well as hard materials are explored and assessed. Current Li-ion batteries utilize C- or Si-based anodes. The cage structures of hybrid carbon clathrates may enable Li storage and promote the development of high capacity anodes for Li-ion battery applications. Lastly, the current status of the synthesis of selected carbon-silicon and carbon–nitrogen clathrates are reported and their challenges are discussed, followed by summary and conclusions.

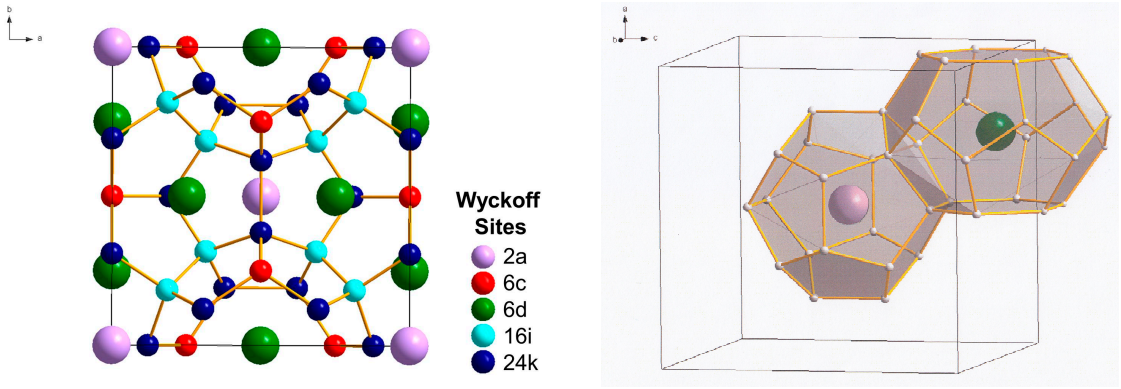

(a) (b)

Figure 1. Crystal structure of Type I C_{46} clathrate (SG: $Pm\bar{3}n$, No. 223): (a) unit cell and (b) cage structure depicting the two building polyhedrons consisting of two nano-cages of 20 atoms (C_{20} cage) and 24 atoms (C_{24} cage). The nano-cages are formed of carbon atoms occupying the following Wyckoff positions identified with different colors: C(1) 6c (red), C(2) 16i (light blue) and C(3) 24k (dark blue). The Li guest atoms inserted inside the cages occupy the positons Li(1)2a (light purple) and Li(2) 6d (green). (Color online: version: the different Wyckoff positions are identified with different colors.)

2. Carbon Clathrates

Type I carbon clathrate, C_{46}, is comprised of a framework of C atoms forming a 3D cage structure in sp^3 bonding [5]. The unit cell of C_{46} is depicted with the positions of the Wyckoff sites in Figure 1(a), while the cage structure is shown in Figure 1(b). Type I carbon clathrate, C_{46}, consists of 46 sp^3 C with a regular arrangement of two 20-atom cages and six 24-atom cages that fused together through five-atom pentagonal rings and occasionally six-atom rings, Figure 1(b). The bond angle of the five-atom pentagonal rings is 108°, while it is 109.49° for the six-atom hexagonal rings [5]. The structures is simple cubic (sc) with a lattice parameter of 6.696 – 6.722 Å and 46 C atoms per unit cell [1, 2]. The crystal structure of C_{46} clathrate belongs to the Space group $Pm\bar{3}n$ and Space Group Number 223 [1, 2]. Type I clathrates can be alloyed by framework substitution and guest atom insertion into the cage structure. For example, some of the framework atoms of a Type I clathrate can be substituted by atom M, while the empty space within the cage structure can serve as host sites for guest atoms A, as shown in Figure 1(b). There are two small cages that can host two guest atoms at the Wyckoff 2a sites and there are six large cages that can host six atoms at the Wyckoff 6d sites without a significant effect on the unit cell volume. Type I alloyed carbon clathrates can be described by the formula: $A_xM_yC_{46-y}$ [1, 3, 4], where A and M represent the guest and substitution atoms and x and y represent the number of guest and substitution atoms, respectively. Representative C framework and Li guest atoms at Wyckoff 2a and 6d sites are shown in Figure 1(b). The structure of Type II carbon clathrate (C_{136}) is comprised of four C_{20} cages and two C_{28} cages that are fused together through six-atom hexagonal rings. It has a face-centered cubic structure (fcc) belong to the space group Fd3m with 34 atoms per unit cell or 136 atoms per supercell. The lattice parameter of C_{136} is about 9.647 – 9.689 Å, as tabulated in Table 1 [2]. The hexagonal carbon clathrate (hcp-C_{40}) is comprised of three C_{20}, two C_{24}, and two C_{26} cages; it belongs to the space group P6/mmm

Preprints (www.preprints.org) | NOT PEER-REVIEWED | Posted: 18 January 2018 doi:10.20944/preprints201801.0166.v1

Peer-reviewed version available at C 2018, 4, 7; doi:10.3390/c4010007

with 40 atoms per unit cell. The lattice parameters of Type I, Type II, hexagonal carbon, graphite, and diamond are compared in Table 1 [2].

Table 1. Calculated equilibrium volume (V_0 in Å^3/atom) and lattice parameters (a_0, c_0 in Å), cohesive energy (E_{coh}), and energy of formation (ΔE_f) for fcc-C_{136}, sc-C_{46}, hcp-C_{40}, diamond, and graphite at zero pressure, compared to available experimental data for diamond graphite and calculated data for C_{46} and C_{136}. Modified from Wang et al. [2].

Structure	Method	V_0 (Å^{3}atom)	a_0 (Å)	c_0 (Å)	E_{coh}, eV/atom	ΔE_f, eV/atom
fcc-C_{136}	VASP[a] [2][a]	6.601	9.647		-7.709 [2]	0.074
	DMOL[b] [6][b]	6.688	9.689	N.A.	-7.263 [6]	0.087
	CPMD [5][c]	–	–	–	–	0.07
sc-C_{46}	VASP [2]	6.543	6.702	N.A.	-7.677 [2]	0.106
	DMOL [6]	6.604	6.722	N.A.	-7.235	0.115
	VASP [11]	6.526	6.696	N.A.	–	0.09
	VASP [15]	–	6.6973	–	–	0.08
	CPMD [15]	–	6.7138	–	–	0.14
	CPMD [5]	–	–	–	–	0.09
	CRYSTAL95 [12][d]	6.259	6.7029	–	–	0.20 [3]
hcp-C_{40}	VASP [2]	6.609	6.695	6.809	-7.656	0.127
	DMOL [6]	6.697	6.725	6.839	-7.213	-0.013
Diamond	VASP [2]	5.705	3.574		-7.783	0
	DMOL [6]	5.787	3.591	N.A.	-7.350	0
	Expt. [13, 14]	5.673	3.567		-7.20	0
Graphite	VASP [2]	8.878	2.470	6.721	-7.916	-0.133
	DMOL [6]	8.983	2.479	6.747	-7.516	-0.166
	Expt. [13, 14]	8.803	2.662	6.708	-7.40	-0.20

a: Vienna Ab-initio Simulation Package (VASP) code [19]
b: Density Functional Calculations on Molecules (DMOL) [6]
c: Car-Parrinello Molecular Dynamic (CPMD) code [16, 17]
d: CRYSTAL95 code [12]

Hypothetical carbon clathrates were first investigated by Nesper et al. [5], who used density functional theory (DFT) to examine cage-like structures that can be derived from zeolites or related to the zeolite topology. Most of the compounds investigated by Nesper et al. exhibit higher formation energy compared to that of carbon with diamond structure, but carbon clathrate I and II exhibit only slightly higher formation energies than diamond. Benedek et al. [6] identified fcc-C_{34}, hcp-C_{40}, and sc-C_{46} as the first three periodic lattices in a series of polyhedric sp^3 carbon networks that are formed under the topological restrictions of fourfold coordination comprised of only five or six fold rings. A theoretical study of the phase stability of carbon clathrates at high pressures revealed that fcc-C_{138} (Type II) and sc-C_{46} (Type I) are, respectively, the third and fourth most stable carbon phase after diamond and graphite [2]. A pressure-induced phase transition from graphite to fcc-C_{138} is predicted to occur at around a pressure of 17 GPa, and about 21 GPa for C_{46}. Additional carbon compounds at higher energy states include those of hcp-C_{40} and M-carbon [2]. Ker et al. [7] suggested small atoms such as Li and Be may be intercalated into the cages of Type I carbon clathrates in order to enhance phase stability. First-principles computations by Bernasconi et al. [8] showed that hcp-C_{40} is suitable to be *n* doped by Li insertion and *p* doped by substitutional B. Theoretical computations by Rey et al. [1] showed that Li atoms can indeed be intercalated into the small cages of C_{46} to form Li_8C_{46}, but the energy of formation of the lithiated compound is increased compared to the unlithiated C_{46} [1]. These investigators also showed that the minimum energy barriers for attaining the C_{46} and Li_8C_{46} may be reached at a pressure close to 40 GPa, suggesting that these metastable phases may be synthesized under extreme conditions of high pressure and temperature [1]. Reported synthesis of 3D cage-like covalent crystals such as C_{20} [9], C_{36} [10], and

Preprints (www.preprints.org) | NOT PEER-REVIEWED | Posted: 18 January 2018 doi:10.20944/preprints201801.0166.v1

Peer-reviewed version available at C 2018, 4, 7; doi:10.3390/c4010007

traces of other compounds like C_{60} and C_{70} [10, 11], suggests that the high-temperature and high-pressure route might be a viable processing method. Unfortunately, no carbon clathrates have been synthesized so far. The bonding type (i.e., sp^3 or sp^2) of some of these carbon clusters has not been characterized or positively identified.

3. Hybrid Carbon-Silicon Clathrates

To overcome the difficulties associated with synthesizing carbon clathrates under extreme conditions, Chan et al. [15] considered the use of first-principles methods to identify appropriate small-sized atoms that were amenable to the formation of new silicon-based clathrate compounds for energy storage and/or harvesting applications. This approach was motivated by the recognition that silicon clathrates are readily synthesized by conventional processing methods. As such, a clathrate with a hybrid carbon-silicon framework may be more amenable to conventional processing than that of a carbon framework. Thus, a series of Type I hybrid carbon-silicon compounds was designed by substituting some of the Si atoms on the Si_{46} framework with C atoms in order to identify the potential hybrid carbon-silicon clathrate compounds that exhibit favorable energy of formation for synthesis by conventional methods. First-principles computations were performed by Chan et al. [15] based on the Car-Parrinello Molecular Dynamics (CPMD) code [16, 17] to investigate the effects of carbon substitution on a Si_{46} framework. These calculations indicates that carbon atoms can partially substitute Si atoms on the Si_{46} framework to form a metastable hybrid silicon-carbon clathrate, which can be represented by the chemical formula C_ySi_{46-y}. Figure 2(a) shows a representation of the Type I C_ySi_{46-y} clathrates. Furthermore, guest atoms can be inserted into the cage structure to stabilize the hybrid silicon carbon clathrate by reducing the energy of formation to form a class of new hybrid silicon and carbon clathrates, represented as $A_xC_ySi_{46-y}$. These hybrid structures do not exist in nature and, thus, represent a novel structure of matter**.** Figure 2(b) shows a structural representation of the Type I $A_xC_ySi_{46-y}$ clathrate compounds. The computed values of the energy change of formation per atom for selected $Ba_8C_ySi_{46-y}$, C_{46}, $C_{40}Si_6$, and $C_{23}Si_{23}$ are compared with those for Si_{46} and Ba_8Si_{46} in Figure 3. The minima of the energy change curves of these $Ba_8C_ySi_{46-y}$ clathrate compounds are positive, indicating that these compounds are metastable.

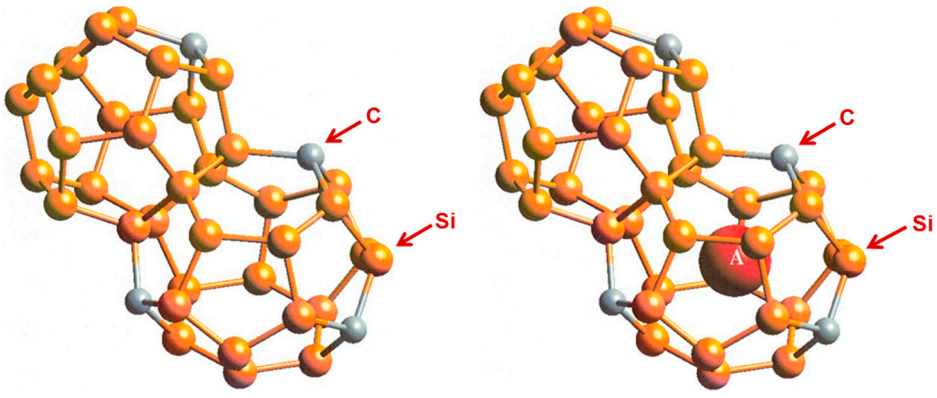

(a) (b)

Figure 2. Cage structure of Type I carbon-silicon clathrate,C_ySi_{46-y}, (a) without guest atoms and (b) with x number of guest atoms A resided within the cage. From Chan et al. [15].

Preprints (www.preprints.org) | NOT PEER-REVIEWED | Posted: 18 January 2018 doi:10.20944/preprints201801.0166.v1

Peer-reviewed version available at C 2018, 4, 7; doi:10.3390/c4010007

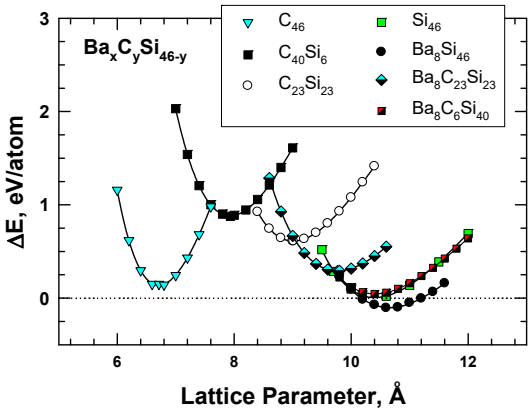

Figure 3. Energy changes curves for selected Type I clathrate compounds of $Ba_8C_ySi_{46-y}$, C_{46}, $C_{40}Si_6$, and $C_{23}Si_{23}$ compared against those of Si_{46} and Ba_8Si_{46}. From Chan et al. [15].

The role of guest atoms on the energy of formation (ΔE_f) of hybrid carbon-silicon clathrates was investigated by placing guest atoms A such as Li, K, Na and Ba into the cage structure. Results of the energy calculation for this series of hybrid carbon-silicon clathrates are presented in Figure 4, which shows that several hybrid carbon-silicon clathrates exhibit relatively low ΔE_f values. The $A_xC_6Si_{40}$ clathrates are of interest because the values of the energy of formation are only slightly positive and less than 0.3 eV. Furthermore, the lattice parameter of these Type I clathrates can be reduced upon judicious selection of the guest atoms.

Variants of the $A_xC_ySi_{46-y}$ clathrates are $A_xE_{8-x}C_yAl_zSi_{46-y-z}$ which are alloyed with multiple guest atoms (A and E), and substitution atoms (C and Al). Al substitution was considered because a previous study [18] reported that Al-substituted Si clathrates were stable and amenable to processing by conventional vacuum arc-melting techniques. Figure 4 shows lattice parameters for Al and C substitution on the framework with Ba, Li, and K doping. Compared to the Si_{46}, Al substitution resulted in a slight expansion of the framework as the equilibrium lattice, is shifted to a larger value for the lattice parameter, while C substitution reduced the lattice parameter. Ba, K, and Li insertion stabilize the C-, and Al-substituted framework by virtue of a negative value for the energy change. In addition, the equilibrium lattice constant and the framework size can be decreased by insertion of alkaline atoms, as shown in Figure 4, for $Li_8C_6Al_{10}Si_{30}$ and $Ba_2Li_6C_6Al_{10}Si_{30}$.

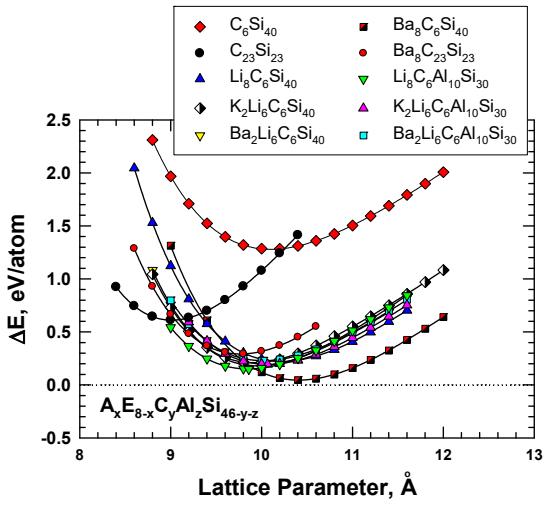

Figure 4. Computed energy change curves for various C-substituted Type I silicon clathrate frameworks with and without Li, Na, K, and Ba guest atoms. From Chan et al. [15].

Preprints (www.preprints.org) | NOT PEER-REVIEWED | Posted: 18 January 2018 doi:10.20944/preprints201801.0166.v1

Peer-reviewed version available at C 2018, 4, 7; doi:10.3390/c4010007

The CPMD results were utilized to establish a correlation between the energy of formation and the lattice parameter for hybrid carbon-silicon clathrates, $A_xC_ySi_{46-y}$, with guest atoms, A, which include alkaline metals such as Li, Na, K, and Ba. The correlation, shown in Figure 5(a), indicates that the alkaline guest atoms generally lower the energy formation but increase the lattice constant of the hydride clathrates. Figure 5(a) depicts that all of the carbon-substituted silicon clathrates exhibit positive values of energy of formation, indicating that these clathrate compounds are metastable. Figure 5(a) also shows that the trend line deviates from C_{46}. To validate the CPMD computations, energies of formation for the same series of hydride clathrates were computed using the Vienna Ab-initio Simulation Package (VASP) code [19]. These two sets of energy of formation computations for $A_xC_ySi_{46-y}$ are compared in Figure 5(b), which shows that in general, there is good agreement between the CPMD and VASP computations, including the energy of formation for C_{46}. One source of the discrepancies between VASP and CPMD computations for $C_{40}Si_6$ has been identified to arise from the slight differences in the relaxed atom positions. As the number of carbon atoms in the framework increases, the VASP results for the carbon-rich clathrates tend to deviate from the trend and lean toward C_{46}. Nonetheless, a gap remains between C_{46} and carbon-rich clathrates such as $C_{42}Si_4$ and $C_{40}Si_6$. The finding suggests that the energy and lattice parameters of $C_{46-x}Si_x$ increases rapidly when x is in the range of $1 < x < 4$. In addition, the computed value of the energy of formation is sensitive to the relaxed atom positions.

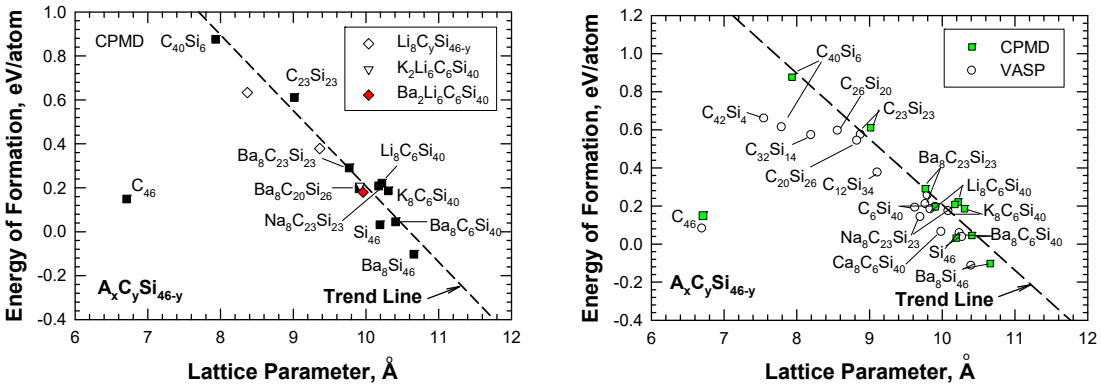

(a) (b)

Figure 5. Energy of formation computed via CPMD and VASP for various intermetallic clathrates based on the $A_xC_ySi_{46-y}$ compositions with the hybrid C_ySi_{46-y} framework: (a) CPMD computations, and (b) comparison of CPMD and VASP computations. From Chan et al. [15].

4. Hybrid Carbon-Nitrogen and Carbon-Boron Clathrates

4.1 Hybrid Carbon-Nitrogen Clathrates

First-principles computational studies by Chan et al. [20] using the Car-Parrinello Molecular Dynamics (CPMD) code [16, 17] indicate that hybrid carbon-nitrogen clathrates may be produced by replacing the carbon atoms in the C_{46} framework with nitrogen atoms to form a hybrid carbon-nitrogen framework, which can be represented by N_yC_{46-y}. Figure 6(a) shows a depiction of the Type I N_yC_{46-y} clathrates. Furthermore, guest atoms can be inserted into the cage structure to stabilize the hybrid nitrogen-carbon clathrate by reducing the energy of formation. This class of nitrogen-substituted carbon clathrates can be represented as $A_xN_yC_{46-y}$. Figure 6(b) shows a structural depiction of Type I $A_xN_yC_{46-y}$ clathrate with a Li guest atom.

The influence of Li guest atom (A = Li) on the structural stability of the hybrid C-N framework was considered by Chan et al. [20]. Figure 7(a) shows that insertion of Li atoms lowers the energy formation and at the same time expands the framework for Li atoms ranging from 2 to 48. Table 2 summarizes the computed lattice constants and energy of formations for individual Type I clathrate compounds. In addition, the computed values of the energy of formation per atom for C_{46}, N_yC_{46-y-z},

Preprints (www.preprints.org) | NOT PEER-REVIEWED | Posted: 18 January 2018 doi:10.20944/preprints201801.0166.v1

Peer-reviewed version available at C 2018, 4, 7; doi:10.3390/c4010007

and $Li_xN_yC_{46-y}$ are compared in Figure 7(b). The results in Figure 7(b) show that nitrogen substitution can lower the energy of formation of N_yC_{46-y} relative to that for C_{46}. Furthermore, Li insertion reduces the energy of formation of $Li_xN_yC_{46-y}$ clathrates to negative values, which indicates that these compounds are more stable than C_{46}.

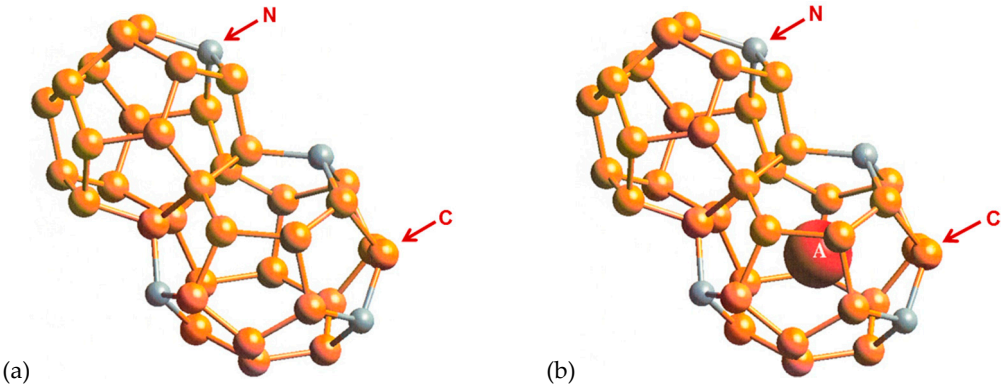

Figure 6. Cage structure of Type I nitrogen-carbon clathrate, N_yC_{46-y}, with and without guest atoms: (a) empty N_yC_{46-y}, and (b) ($A_xN_yC_{46-y}$) with x number of guest atom A resided within the cage. From Chan et al. [20].

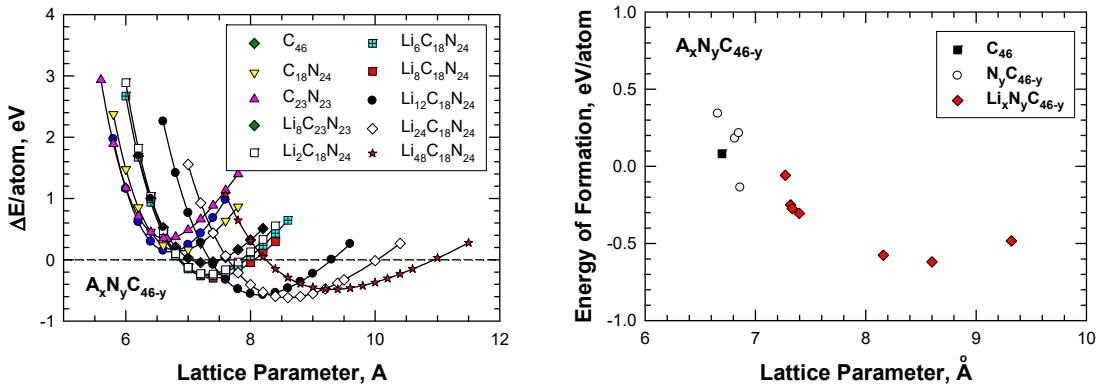

Figure 7. Comparisons of computed energy curves and energy of formation for Type I C_{46}, N_yC_{46-y}, and $A_xN_yC_{46-y}$ with various amounts of Li guest atoms as a function of lattice parameter: (a) energy change curve, and (b) energy of formation. From Chan et al. [20].

Table 2. Summary of computed lattice constant, a_o, and energy of formation, ΔE_f, for Type I carbon clathrate compounds. From Chan et al. [20].

Compound	a_o, Å	ΔE_f, eV/atom
C_{46}	6.6973	0.0815
$C_{18}N_{24}$	6.8622	-0.1377
$C_{19}N_{27}$	6.8148	0.1803
$C_{20}N_{26}$	6.8502	0.2144
$C_{23}N_{23}$	6.6596	0.3416
$Li_2C_{18}N_{24}$	7.3192	-0.25
$Li_6C_{18}N_{24}$	7.3336	-0.2742
$Li_8C_{18}N_{23}$	7.3979	-0.3051
$Li_8C_{23}N_{23}$	7.2716	-0.0578
$Li_{12}C_{18}N_{24}$	8.1592	-0.5765
$Li_{24}C_{18}N_{24}$	8.6003	-0.6192
$Li_{48}C_{18}N_{28}$	9.3206	-0.4832

Preprints (www.preprints.org) | NOT PEER-REVIEWED | Posted: 18 January 2018 doi:10.20944/preprints201801.0166.v1

Peer-reviewed version available at C 2018, 4, 7; doi:10.3390/c4010007

4.2 Hybrid Carbon-Boron Clathrates

Using VASP [19], Zeng et al. [21] computed the energy of formation and band gaps for five different Li-filled, B-substituted carbon clathrates, including $Li_8C_{38}B_8$ (Type I), $Li_6C_{28}B_6$ (Type II), $Li_7C_{33}B_7$ (Type IV), $Li_2C_{10}B_2$ (Type VII), and $Li_6C_{28}B_6$ (Type H) at the ground state. A range of strategies has been utilized to determine the energetics of replacing selected carbon atoms on the framework with boron substitution atoms and Li insertion in order to achieve a lower enthalpy and a more stable clathrate compound. These strategies included crystal symmetry, charge distribution, strengthening bonding, relieving bond angle, and reducing lattice strain. Based on these strategies, a representative low-enthalpy Li-doped, B-substituted candidate for each type of the five clathrates has been identified. Several energetically competitive structures, however, exist for each clathrate type. These authors concluded that B substitution stabilizes the cage structure and lowers substantially the energy cost for inserting Li atoms into the clathrate cages to about -2eV/Li at 1 atom pressure [21]. In addition, all five carbon clathrates display a semiconducting electronic structure. Li doping of the B substituted carbon clathrates reduced the band gaps of the carbon clathrate compounds to the 0.6 to 2.9 eV range [21].

Zeng et al. [21] also investigated theoretically two possible competing routes for synthesizing $Li_xC_yB_x$: (1) formation of LiBC, and (2) introduction of C-vacancies. The authors indicated that LiBC formation is thermodynamically feasible but the process may be kinetically limited due to structural differences between LiBC and $Li_xC_yB_x$. The C-vacancy route, on the other hand, may be a costly process for stabilizing Li insertion in comparison to B substitution of the carbon framework. Because of kinetic constraints, the authors suggested that some of the $Li_xC_yB_x$ clathrates may exist in amorphous forms.

5. Potential Applications of Hybrid Carbon Clathrates

5.1. Hybrid Carbon-Silicon Clathrates as Hydrogen Storage Materials

In an investigation focused on identifying new Si-based clathrates that may be suitable for use as hydrogen storage materials in transportation applications, Chan et al. [22] applied the VASP code [19] to compute the binding energy of hydrogen molecules in selected Type I Si-based and hybrid carbon-silicon clathrates. Si-based intermetallic clathrates were designed in two ways: (1) with or without an alkali-metal guest atom (Na, Li, or Ba) in the cage structure, and (2) substitution of the Si framework with other atoms inserted such as C, Al, and Cu, in order to tune the void space inside the cage structure for maximum H_2 capacity and optimum binding interactions. The DFT results of the binding energy in eV/H_2 for hydrogenation of Si_{46}, C_6Si_{40}, $Na_8Al_8Si_{38}$ and $Li_8Al_8Si_{38}$ are presented in Figure 8(a) as function of gravimetric capacity in weight percentage converted from the number of H_2 molecules inserted in the cage structure. The desirable binding energy range for H_2 at ambient temperature is also superimposed as dashed lines in Figure 8(a). The results indicate that the binding energy between hydrogen molecules and the interstitial cavities of Si_{46} and C_6Si_{40} cage structures increases with the number of H_2 molecules inserted or gravimetric capacity. Figure 8(a) shows that $Na_8Al_8Si_{38}$ and $Li_8Al_8Si_{38}$ exhibit hydrogen binding interactions that are within the desirable range for the entire range of gravimetric capacity considered, ranging from 8 to 128 H_2 molecules inserted. On this basis, this finding suggests that $Na_8Al_8Si_{38}$ and $Li_8Al_8Si_{38}$ show high physisorption capacity for H_2 with suitable binding energy values as potential hydrogen storage materials at or near ambient temperatures. The lattice parameters for Si_{46}, C_6Si_{40}, $Na_8Al_8Si_{38}$, and $Li_8Al_8Si_{38}$ after various levels of hydrogenation are shown in Figure 8(b) as a function of gravimetric capacity. The lattice parameter for hydrogenated $Na_8Al_8Si_{38}$, and $Li_8Al_8Si_{38}$ increase with increasing number of hydrogen molecules inserted (gravimetric capacity), while those of hydrogenated Si_{46} and C_6Si_{40} do not exhibit similar increases with gravimetric capacity. For comparison purposes, Figure 8(b) also shows the system-level storage targets for gravimetric and volumetric capacity prescribed by the U.S. Department of Energy (DOE) for on-board storage on vehicles for 2020 and the ultimate fleet targets [23].

Preprints (www.preprints.org) | NOT PEER-REVIEWED | Posted: 18 January 2018 doi:10.20944/preprints201801.0166.v1

Peer-reviewed version available at C 2018, 4, 7; doi:10.3390/c4010007

Figure 9 presents the results of the lattice parameters for hydrogenated Si_{46}, C_6Si_{40}, $Na_8Al_8Si_{30}$ and $Li_8Al_8Si_{38}$ as a function of volumetric capacity. From Figure 9, it appears that both the hybrid carbon and silicon clathrates (i.e., Si_{46}, C_6Si_{40}, $Na_8Al_8Si_{30}$ and $Li_8Al_8Si_{38}$) might be considered promising storage materials exhibiting volumetric capacities that may achieve or exceed the DOE targets for vehicles for 2020 and beyond. Moreover, the Ba-, Na-, and Li-stabilized alloyed clathrates exhibit larger lattice parameters and expand to a greater extent compared to hydrogenated Si_{46} and C_6Si_{40} at equivalent volumetric capacity. This finding suggests that a framework structure with a large lattice parameter may be beneficial for increasing the volumetric capacity of hydrogen storage. A number of hybrid Type I carbon silicon clathrates with large lattice constants have been identified in Figure 5. Unfortunately, the hydrogen storage capabilities of these hybrid clathrates have not been evaluated or assessed. By virtue of large lattice constants, Type II carbon-based clathrates might also have suitability for hydrogen storage, but their hydrogen storage capacities have, so far, not been investigated.

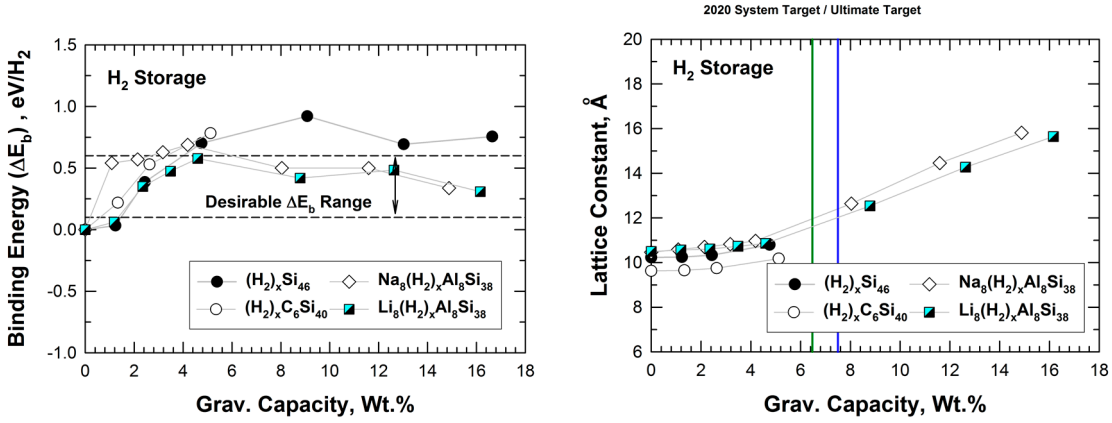

(a) (b)

Figure 8. Predicted internal binding energy, lattice constant, and gravimetric capacity of Si_{46}, C_6Si_{40}, $Na_8Al_8Si_{38}$, and $Li_8Al_8Si_{38}$. The range over which binding interactions of H_2 is favorable for room-temperature storage is noted as dashed lines: (a) binding energy vs gravimetric capacity, and (b) lattice constant vs. gravimetric capacity. From Chan et al. [22]. The vertical green line indicates DOE's 2020 system target, while the vertical blue line indicates the DOE ultimate fleet target for on-board storage on vehicles.

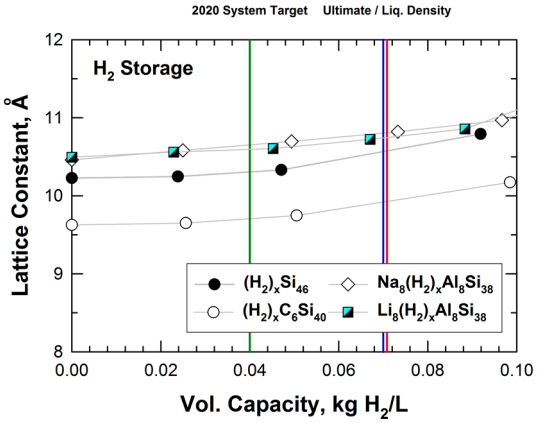

Figure 9. Predicted volumetric capacity and lattice constant for intermetallic clathrates of Si_{46}, C_6Si_{40}, $Na_8Al_8Si_{38}$, and $Li_8Al_8Si_{38}$. Vertical lines mark the system level targets prescribed by DOE for on-board storage on vehicles. From Chan et al. [22].

5.2. Hybrid Carbon-Silicon Clathrates as Electronic or Electrode Materials

Chan and Peng [24] employed the first principles DFT code VASP [19] to compute the energy of formation and the optimal lattice constants of several hybrid carbon silicon clathrates. In addition, they also computed the electronic structures including the band structure, density of states (DOS), the spd- and site-projected partial density of states (PDOS) of the selected materials. Geometry optimization and self-consistent total energy calculations were performed using the PBE functional [25] and projector-augmented wave (PAW) [26, 27] potentials along with the plane wave basis sets. Besides the PBE functional [25], the Hyed-Scuseria-Ernzerhof (HSE) screened Coulomb hybrid density functional [28] was also utilized to predict the energy band gap for Si_{46} in order to gain a perspective on potential underestimations in the PBE band gap results. Detailed descriptions of the computational methods and results can be found in Chan and Peng [24].

Figure 10 compares the electronic band structure of Si_{46}, C_6Si_{40}, $C_{12}Si_{34}$, and $C_{23}Si_{23}$. The Fermi level is set at zero eV (i.e. the top edge of valence band). For Si_{46}, a relatively large band gap is (E_g = 1.31 eV) observed between the Fermi level and the lower edge of the conduction band. The band gap is reduced to E_g = 0.44 eV in C_6Si_{40} when 6 Si atoms on the framework are replaced by C atoms. Compared to Si_{46}, the band gap is reduced to E_g = 0.63 eV when the substituted C atoms are increased to 12 in $C_{12}Si_{34}$. Further substitution of Si by C in the framework causes the energy band gap to increase to 1.2 eV, 1.67 eV, and 2.64 eV in $C_{23}Si_{23}$, $C_{34}Si_{12}$, and $C_{40}Si_6$, respectively. For C_{46}, the band gap is 3.87 eV, which represents an increase of 2.56 eV compared to Si_{46}. Thus, the hybrid carbon-silicon framework exhibits the lowest band gap when the number of substituted carbon atoms on the framework ranges from 6 to 12.

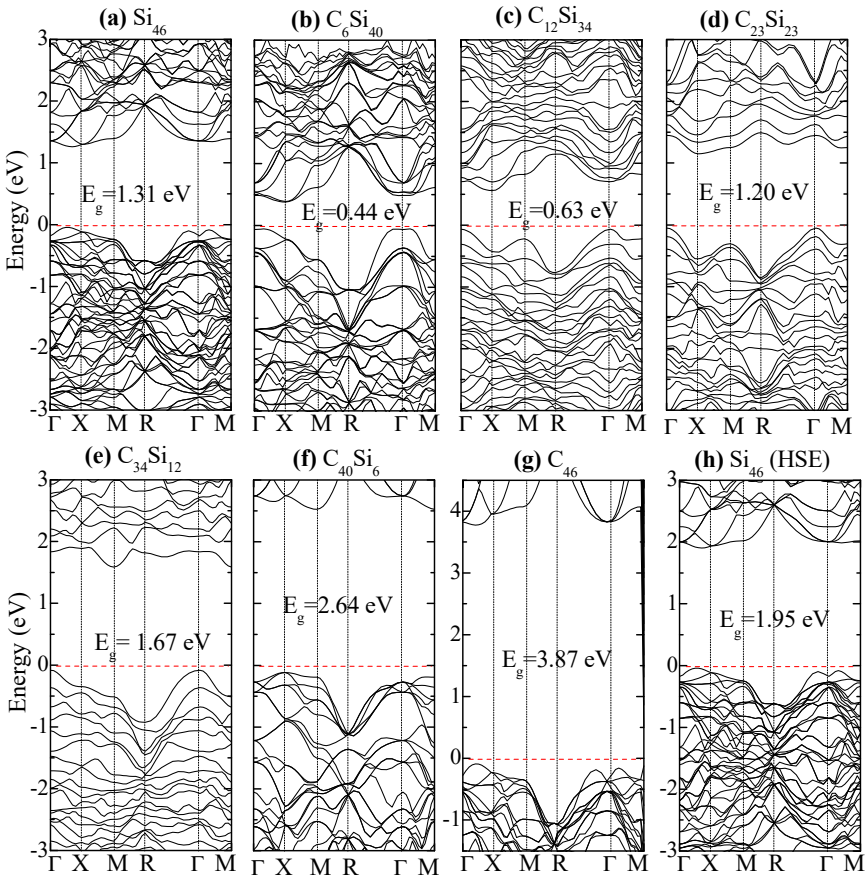

Figure 10. Electronic band structures of (a) Si_{46}, (b) C_6Si_{40}, (c) $C_{12}Si_{34}$, (d) $C_{23}Si_{23}$, (e) $C_{34}Si_{12}$, (f) $C_{40}Si_6$, (g) C_{46} predicted by DFT. (h) presents the band structure of Si_{46} predicted using the HSE hybrid functional. The corresponding band gaps are denoted. The Fermi level is referenced at the top of valence band at zero. From Chan and Peng [24].

Preprints (www.preprints.org) | NOT PEER-REVIEWED | Posted: 18 January 2018 doi:10.20944/preprints201801.0166.v1

Peer-reviewed version available at C 2018, 4, 7; doi:10.3390/c4010007

The total and partial DOS of Si_{46}, C_6Si_{40}, $C_{23}Si_{23}$, and $C_{40}Si_6$ are compared in Figure 11 with the Fermi level shown by the dashed-dotted line at zero eV. Figure 11(a) shows that the p-electrons of Si contribute to the edges of the valence and conduction bands to form the band gap in Si_{46}. In Figure 11(b), a significant contribution of the s-electrons of substituted C atoms to the bottom of the conduction band and lowers the band gap of C_6Si_{40}. As the number of substituted C atoms per formula unit increases to 23, the conduction bands of $C_{23}Si_{23}$ are dominated by both the C-p electrons and Si-p electrons; as a result, the band gap is widened again, as shown in Figure 11(c). A further widening of the band gap in $C_{40}Si_6$ is presented in Figure 11(d).

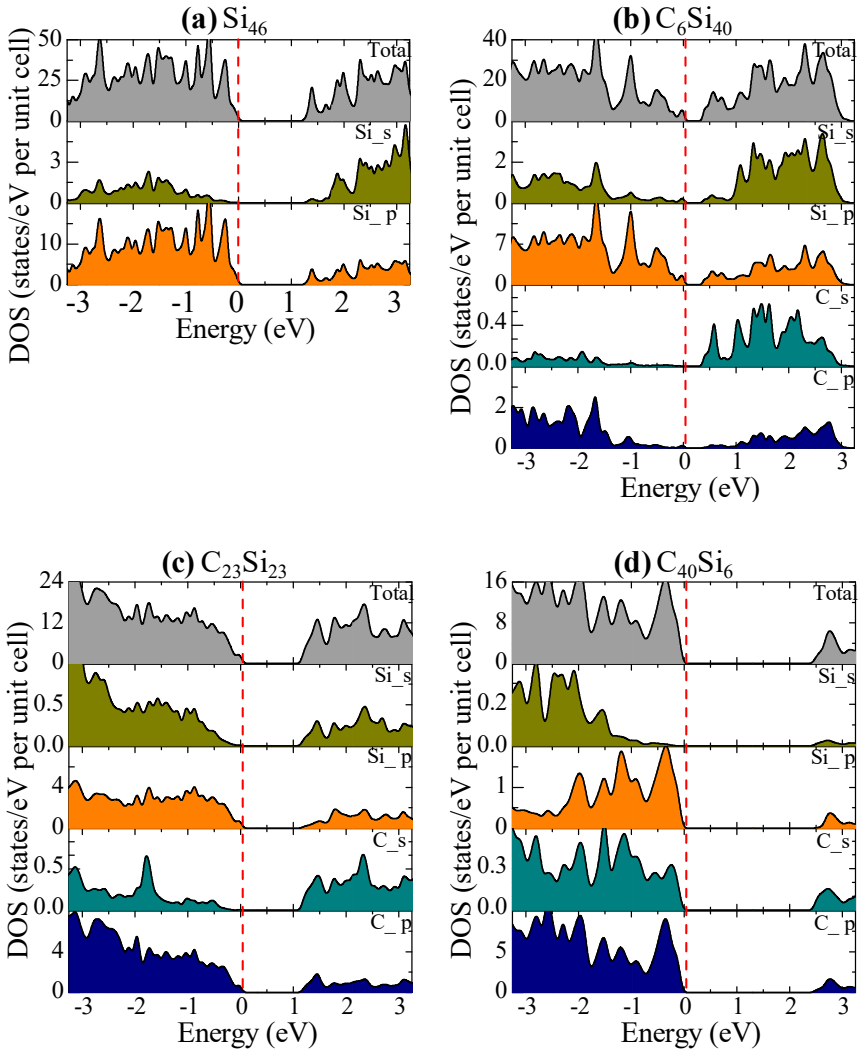

Figure 11. The total and *s*-, *p*-orbital projected density of states of (a) Si_{46}, (b) C_6Si_{46}, (c) $C_{23}Si_{23}$ and (d) $C_{40}Si_6$. The Fermi level is referenced at the top of valence band at zero. From Chan and Peng [24].

The band gap of the hybrid carbon-silicon clathrates is influenced by the number of substitution C atoms on the framework, as illustrated in Figure 12. Substitution of Si atoms on the Si_{46} framework by C atoms progressively reduces the band gap due to the interaction of C valence electrons with the Si conduction band. The band gap is reduced with increasing numbers of C atoms on the hybrid Si-C framework when the number of carbon atoms is about 6 to 12. The band gap is widened again when the number of C is increased above 23. Conversely, a large band gap exists for C_{46} and the band gaps is reduced when the C atoms on the C_{46} framework is substituted by Si atoms. Again, the band gap is reduced with increasing numbers of Si atoms on the hybrid Si-C framework until the number of Si atoms on the framework exceeds 40. A minimum band gap occurs when there are

about 6 to 12 carbon atom occupants per formula unit on the framework and the minimum band gap appears to be about 0.44 eV. The general trend of the results indicates that the band gap of the carbon-silicon clathrate framework can be tuned by adjusting the number of carbon atoms on the framework. Furthermore, a metal conductor can be obtained by dropping Li, Na, K, Mg, Ca, or Ba atoms inside the cage structure of the framework. The wide band gap and tunability make carbon clathrates potential materials for electronic applications.

The hybrid carbon-silicon clathrates may also be considered potential electrode materials for Li-ion batteries. The electronic structure calculations indicate that the empty C_ySi_{46-y} clathrate exhibits a small band gap (0.44 to 0.63 eV) when y, the number of substituted carbon atoms, is in the range of 6 to 12. With this composition range, a small band gap may be induced to provide sufficient electronic conductivity for insertion of lithium ions into the cage structure to proceed when C_ySi_{46-y} clathrate is used as an anode. Once Li ions are inserted, the electronic conductivity of $Li_xC_ySi_{46-y}$ is likely to increase with increasing number of Li ions inserted; subsequently, the lithiated C_ySi_{46-y} clathrate may become a metal-like conductor when 8 or more Li ions are inserted [24]. Recent works by Li et al. [29] and Chan et al. [30, 31] have shown that lithiation of $Ba_xAl_ySi_{46-y}$ and empty Si_{46} clathrates are feasible even in the presence of Ba atoms occupying some of the sites within the cage structure of $Ba_xAl_ySi_{46-y}$. Thus, it is possible that some of C_ySi_{46-y} clathrates doped with the alkaline metals (Na, K) or alkaline earth metals (Ba, Ca, Mg) may be lithiated and serve as potential electrode materials for Li-ion batteries. There are more empty spaces within the cage structure of C_ySi_{46-y} compared to those in graphite or carbon-based nanomaterials [32]. On this basis, C_ySi_{46-y} anodes may accommodate more Li storage capacity than conventional graphite anodes or carbon-based nanomaterials [32]. In conventional Si anodes, Li storage is accompanied by formation of various LiS_x silicides. Reaction with Li with C_ySi_{46-y} anodes to form various forms of LiC_x or $LiSi_x$ compounds [32, 33] may provide additional Li storage mechanisms, but it would likely destroy the clathrate structure and limits the overall capacity or mechanical performance.

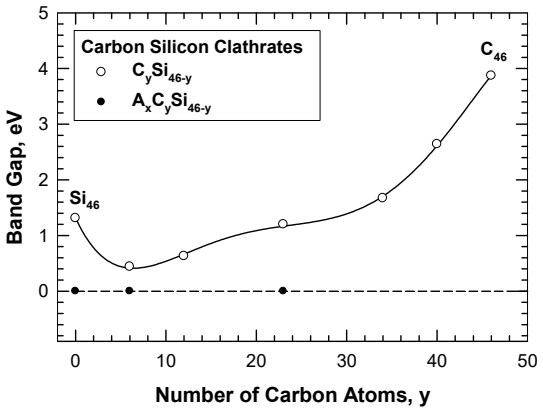

Figure 12. Computed band gap of C_ySi_{46-y} as a function of number of C atoms on the hybrid carbon-silicon framework. The band gap is at a minimum at about C = 6. From Chan and Peng [24].

5.3. Hybrid Carbon-Nitrogen Clathrates as Hard Materials

To explore the potential of N_yC_{46-y} as hard materials, the bulk modulus of the various intermetallic clathrate compounds was computed by Chan et al. [20] using the first-principles approach according to the expression given by [34]

$$\frac{\Delta E}{V} = \frac{9}{2} B \delta^2 , \quad (1)$$

where ΔE/V is the energy change per unit cell volume, B is the bulk modulus, and δ is the normal strain in the three principal directions of the unit cell. To obtain the bulk modulus, $\Delta E/V$ values were computed as a function of the normal strain δ. The $\Delta E/V$ data were plotted versus δ for each deformed unit cell of individual clathrate compounds. The data were then fitted to Eq. (1) and the

Preprints (www.preprints.org) | NOT PEER-REVIEWED | Posted: 18 January 2018 doi:10.20944/preprints201801.0166.v1

Peer-reviewed version available at C 2018, 4, 7; doi:10.3390/c4010007

regression coefficient was then used to obtain the bulk modulus, *B*. The theoretical bulk modulus for various intermetallic clathrate compounds is summarized in Table 3.

Table 3 shows a comparison of the theoretical and experimental data (indicated by an asterisk) of bulk modulus for diamond, carbon nitride, silicon nitride, and silicon carbide from the literature [1-3, 35-39]. The results in Table 3 indicate that a wide range of bulk modulus (from 63 GPa to 400 GPa) can be obtained from Type I hybrid C-N, N-Si, and C-Si clathrates, depending on the framework atoms. Some of the carbon clathrate compounds exhibit bulk moduli that are in the range of 245 GPa to 374 GPa, which are not as high as diamond C or β-C_3N_4, but are comparable to silicon nitride (c-Si_3N_4) and carbon nitride. On this basis, carbon clathrates may be considered for potential applications as hard materials.

Table 3. Computed values of the bulk modulus of selected Type I clathrates compared to theoretical and experimental values of the bulk modulus of diamond, carbon nitride, silicon nitride, and silicon carbide from the literature. Experimental values are indicated by an asterisk (*). From Chan et al. [20].

Compound	Structure	B, GPa
C_{46}	Type I Clathrate (Simple cubic)	373.7 371 [1] 363.7 [2] 409 [3]
$C_{18}N_{24}$	Type I Clathrate	257.35
$C_{23}N_{23}$	Type I Clathrate	311.6
$Li_8C_{23}N_{23}$	Type I Clathrate	245.18
$Si_{23}C_{23}$	Type I Clathrate	124.03
Si_6C_{40}	Type I Clathrate	196.8
$Si_{18}N_{24}$	Type I Clathrate	96.08
$Si_{23}N_{23}$	Type I Clathrate	114.13
C_6Si_{40}	Type I Clathrate	62.9
C (Diamond)	Diamond cubic	438.8 [35] 442* [36]
α-C_3N_4	Hexagonal	378.7 [35]
β-C_3N_4	Cubic spinel	419.1 [36]
c-Si_3N_4	Cubic spinel	300 [37] 300*[38]
SiC	Cubic (Zinc blend)	225* [39]

6. Synthesis of Hybrid Carbon Clathrates

6.1. Hybrid carbon-silicon clathrates

Syntheses of six candidate carbon-silicon clathrate compounds were attempted by Chan et al. [15]. Table 4 summarizes the target compounds and the produced materials that were selected for syntheses by a vacuum arc-melting method. In particular, all six compositions were packaged and shipped to Sophisticated Alloys, Inc. (Butler, PA) where vacuum arc-melting (VAM) of the candidate alloys was performed. A vacuum arc-melter is comprised an electrode and a crucible containing the materials to be melted in a metal vessel that is brought to a vacuum of < 0.1 Pa. The equipment used for the VAM process is available on the website of Sophisticated Alloys (www.alloys.com). To fabricate the clathrate compounds, the arc-melting process was conducted in

Preprints (www.preprints.org) | NOT PEER-REVIEWED | Posted: 18 January 2018 doi:10.20944/preprints201801.0166.v1

Peer-reviewed version available at C 2018, 4, 7; doi:10.3390/c4010007

an argon atmosphere under a sub-atmospheric pressure. As indicated in Table 4, only some of the predicted Type I clathrates (which included $Ba_8C_6Si_{40}$, $Ba_8C_{20}Si_{26}$, and $Ba_8C_{23}Si_{23}$) have been confirmed by successful syntheses. The as-synthesized products, however, contain mixtures of the targeted compounds and starting materials. Thus, further efforts are needed to improve both the yield and the purity of the arc-melted products. Despite the low yields (16% to 39%), successful synthesis of $Ba_8C_6Si_{40}$, $Ba_8C_{20}Si_{26}$ and $Ba_8C_{23}Si_{23}$ represents a significant accomplishment since these compounds are synthesized for the first time. The success in synthesizing $Ba_8C_6Si_{40}$, $Ba_8C_{20}Si_{26}$, and $Ba_8C_{23}Si_{23}$ by arc-melting may be attributed to the use of SiC in the starting admixture [15]. It is thought that SiC is of a higher energy state that overcomes the energy barrier of reaction and allows the metastable carbon-silicon clathrate compounds to form.

Table 4. Summary of targeted compounds and actual compounds produced by arc-melting. From Chan et al. [15].

Composition	Target Compound	Actual Compounds Produced	Type I Clathrate	Yield, %
1	$Na_2Li_6Al_{10}C_6Si_{30}$	None (all sublimed except Si)	No	0
2	$Li_8Al_{10}C_6Si_{30}$	Si, SiC, and AlLiSi	No	0
3	$Ba_8C_6Si_{40}$	$BaSi_2$, Si, and graphite	No	0
4	$Ba_8C_{20}Si_{26}$	Ba, SiC, $BaSi_2$, Si, and $Ba_8C_{20}Si_{26}$	Yes ($Ba_8C_{20}Si_{26}$)	39
5	$Ba_8C_6Si_{40}$	Ba, SiC, $BaSi_2$, Si, and $Ba_8C_6Si_{40}$	Yes ($Ba_8C_6Si_{40}$)	26
6	$Ba_8C_{23}Si_{23}$	Ba, SiC, $BaSi_2$, Si, and $Ba_8C_{23}Si_{23}$	Yes ($Ba_8C_{23}Si_{23}$)	16

6.2. Hybrid carbon-nitrogen clathrates

Syntheses of $Mg_8C_{18}N_{24}$ and $Ba_8C_{18}N_{24}$ were attempted by vacuum arc-melting of admixture of graphitic carbon nitride (g-$C_3N_{4+y}H_y$) and appropriate metal powder compositions shown in Table 5 [20]. Prior experience in synthesizing hybrid silicon-carbon clathrates [15] suggested that Ba could be effective in stabilizing the hybrid carbon-nitrogen framework and offer a good chance for a successful synthesis of nitrogen-substituted carbon clathrates. The rationale was borne out by the attempt to synthesize $Mg_8C_{18}N_{24}$, which was unsuccessful, and successful synthesis of $Ba_8C_{18}N_{24}$. Powder X-Ray Diffraction (PXRD) of the non-milled $Mg_8C_{18}N_{24}$ powders reveals the absence of any peaks that can be attributed to a Type I clathrate structure. All of the peaks in the PXRD pattern can be identified and attributed to those of the graphitic carbon nitride, MgO, and $MgCN_2$, as presented in Table 5. In contrast, $Ba_8C_{18}N_{24}$ was synthesized by arc-melting appropriate amounts of Ba and graphitic carbon nitride (g-$C_3N_{4+x}H_y$) as the starting materials [20]. Admixtures of Ba and g-$C_3N_{4+x}H_y$ (in the proportion of 20.6 g Ba, and 4.51g of g-$C_3N_{4+x}H_y$ powders) was arc-melted to make about 25.11 g of the product, consisting of $Ba_8C_{18}N_{24}$ plus some amounts of unreacted starting materials. The yield and purity is, however, low and needs further improvement to increase the yield and purity.

Table 5. Summary of targeted compounds and actual compounds produced by arc-melting From Chan et al. [20].

Composition	Target Compound	Actual Compounds Produced	Type I Clathrate
1	$Mg_8N_{18}C_{28}$	MgO, g-C_2N_4, and $MgCN_2$	No
2	$Ba_8N_{18}C_{24}$	Ba, g-C_3N_4, and $Ba_8C_{18}N_{24}$	Yes ($Ba_8C_{18}N_{24}$)

7.0 Summary

This overview summarizes the current status of hybrid carbon-silicon, carbon-nitrogen, and carbon-boron clathrates, which are new classes of Type I carbon-based clathrates that have been identified by first-principles computational methods. These theoretical materials have been designed by substituting atoms on the carbon clathrate framework with Si, N and/or B atoms. Stability of the hybrid framework may be stabilized by inserting alkaline-metal guest atoms within the cavities of the cage structure. Series of hybrid carbon-silicon, carbon-nitrogen, carbon-boron, and carbon-silicon-nitrogen clathrates have been shown to exhibit small positive values of the energy of formation, indicating that they are metastable compounds and may be amenable to fabrication. Theoretical calculations that explore the potential applications of hybrid carbon-based clathrates as energy storage materials, electronic or electrode materials, as well as hard materials are presented. The computational results identify compositions of hybrid carbon-silicon, carbon-nitrogen, and carbon-boron clathrates that may be considered candidate materials for use as either electronic materials, hard materials, electrode materials for Li-ion batteries or as hydrogen storage materials. Fabricating selected hybrid carbon-silicon and carbon-nitrogen clathrates by industrial arc-melting techniques have not been always successful. Major limitations of the current processing techniques are the purity and yield of the products when the candidate materials are successfully synthesized.

One of the current challenges of hybrid carbon clathrates is the development of robust processing methods for synthesizing carbon-silicon, carbon-nitrogen, and carbon-boron clathrates. So far, only an industrial arc-melting method has been attempted to fabricate small quantities of low purity Ba-containing hybrid carbon-silicon and carbon-nitrogen clathrates. Future development should expand the processing routes beyond arc-melting. Solution processing methods based on Hofmann-type elimination-oxidation schemes such as those described by Chan et al. [30] and Guloy et al. [40] may be desirable since they can be scaled up to produce larger quantities of clathrate materials. However it is uncertain that hybrid carbon-silicon, carbon-nitrogen, or carbon-boron clathrates can be produced by solution synthesis methods. Once they are synthesized, the impure hybrid clathrates need to be purified. Development of robust purification routes is another challenge that needs to be overcome in order to advance the field of hybrid carbon-based clathrates.

Acknowledgements: This work was supported by the Internal Research Program of Southwest Research Institute (SwRI). Discussion of this article with Professor Candace K. Chan at Arizona State University is acknowledged. The clerical assistance of Ms. L. Mesa, SwRI, in the preparation of this manuscript is acknowledged.

Author Contributions: K.S. Chan wrote the entire article.

Conflicts of Interest: The author declares no conflict of interest.

References

1. Rey, N.; Muñoz, A.; Rodríquez-Hernández, P.; San Miguel, A. First-principles study of lithium-doped carbon clathrates under pressure. J. Phys.: Condens. Matter 2008, 20(21), 215218, DOI: 10.1088/0953-8984/20/21/215218.
2. Wang, J. T.; Chen, C.; Wang D. S.; Mizuseki, H.; Kawazoe, Y. Phase stability of carbon clathrates at high pressure. J. Appl. Phys. 2010, 107(6), 063507-1 – 063507-4, DOI: 10.1063/1.3359682.
3. Perottoni, C. A.; da Jornada, J. A. H. The carbon analogues of type-I silicon clathrates. J. Phys.: Condens. Matter 2001, 13(26), 5981-5998, DOI: 10.1088/0953-8984/13/26/313.
4. Rogl, P. Formation of clathrates. In Thermoelectrics, Proceedings of the 24th International Conference on Thermoelectrics 2005; ICT 2005, Clemson, South Carolina, USA; IEEE pp. 440-445.
5. Nesper, R.; Vogel, K.; Blöchl, P. E. Hypothetical carbon modifications derived from zeolite frameworks. Angew. Chem. Int. Ed. Engl. 1993, *32*(5), 701-703.
6. Benedek, G.; Galvani, E.; Sanguinetti, S.; Serra, S. Hollow diamonds: stability and elastic properties. Chem. Phys. Lett. 1995, 244(5-6), 339-344, DOI: 10.1016/0009-2614(95)00946-2.

7. Ker, A.; Todorov, E.; Rousseau, R.; Uehara, K.; Lannuzel, F. X.; Tse, J. S. Structure and phase stability of binary zintl-phase compounds: lithium–group 13 intermetallics and metal-doped group 14 clathrate compounds. Chem. Eur. J. 2002, 8(12), 2787-2798.
8. Bernasconi, M.; Gaito, S.; Benedek, G. Clathrates as effective *p*-type and *n*-type tetrahedral carbon semiconductors. Phys. Rev. B 2000, 61(19), 12689-12692, DOI: 10.1103/PhysRevB.61.12689.
9. Iqbal, Z.; Zhang, Y.; Grebel, H.; Vijayalakshmi, S.; Lahamer, A.; Benedek, G.; Bernasconi, M.; Cariboni, J.; Spagnolatti, I.; Sharma, R.; Owens, F. J. Evidence for a solid phase of dodecahedral C_{20}. Eur. Phys. J. B – Condensed Matter and Complex Systems 2003, 31(4), 509-515.
10. Piskoti, C.; Yarger, J.; Zettl, A. C_{36}, a new carbon solid. Nature 1998, 393(6687), 771-774.
11. Yamanaka, S.; Kubo, A.; Inumaru, K.; Komaguchi, K.; Kini, N. S.; Inoue, T.; Irifune, T. Electron conductive three-dimensional polymer of cuboidal C_{60}. Phys. Rev. Lett. 2006, 96(7), 076602, DOI: 10.1103/PhysRevLett.96.076602.
12. Dovesi, R.; Saunders, V. R.; Roetti, C.; Causa, M.; Harrison, N. M. CRYSTAL95 User's Manual, 1996, University of Torino.
13. Furthmüller, J.; Hafner, J.; Kresse, G. *Ab initio* calculation of the structural and electronic properties of carbon and boron nitride using ultrasoft pseudopotentials. Phys. Rev. B 1994, 50(21), 15606-15622.
14. Dresselhaus, M. S.; Dresselhaus, G.; Eklund, P. C. Science of fullerenes and carbon nanotubes, Academic Press, New York, N.Y. USA, 1996.
15. Chan, K. S.; Miller, M. A.; Liang, W.; Ellis-Terrell, C.; Peng, X. First-principles computational design and synthesis of hybrid carbon-silicon clathrates. J Mater Sci. 2014, 49(7), 2723-2733.
16. Car, R.; Parrinello, M. Molecular dynamics: an *ab initio* electronic structure and molecular dynamics program, Version 3.13.1, The CPMD Consortium, June 27, 2008, http://www.cpmd.org.
17. Car, R.; Parrinello, M. Unified approach for molecular dynamics and density-functional theory. Phys. Rev. Lett. 1985, 55(22), 2471.
18. Tsujii, N.; Roudebush, J. H.; Zevalkink, A.; Cox-Uvarov, C. A.; Snyder, G. J.; Kauzlarich, S. M. Phase stability and chemical composition dependence of the thermoelectric properties of the type-1 clathrate $Ba_8A1_xSi_{46-x}$ ($8 \le x \le 15$). J of Solid State Chem 2011, 184(5), 1293-1303.
19. Kresse, G.; Marsman, M.; Furthmüller, J. Vienna *ab-initio* simulation package – VASP the guide, Universität Wien, Wien, Austria, 2012.
20. Chan, K. S.; Miller, M. A.; Liang, W.; Ellis-Terrell, C. Computational design and synthesis of nitrogen-substituted carbon and silicon clathrates. Mater Res Lett. 2014, 2(2), 70-75.
21. Zeng, T.; Hoffmann, R.; Nesper, R.; Ashcroft, N. W.; Strobel, T. A.; Proserpio, D. M. Li-filled, B-substituted carbon clathrates. J. Am. Chem. Soc. 2015, 137, 12639-12652, DOI: 10.1021/jacs.5b07883.
22. Chan, K. S.; Miller, M. A.; Peng, X. First principles computational study of hydrogen storage in silicon clathrates. Material Research Letters 2018, 6(1), 72-78, DOI: 10.1080/21663831.2017.1396261.
23. US Drive Target Explanation Document: Onboard hydrogen storage for light-duty fuel cell vehicles, Department of Energy, Washington, DC, May 2015.
24. Chan, K. S.; Peng, X. First-principles study of electronic structure of type I hybrid carbon-silicon clathrates. Journal of Electronic Materials 2016, 45(8), 4246-4256, DOI: 10.1007/s11664-016-4621-3.
25. Perdew, J. P.; Burke, K.; Ernzerhof, M. Generalized gradient approximation made simple. Phys Rev Lett. 1996, 77(18), 3865-3868.
26. Kresse, G.; Joubert, D. From ultrasoft pseudopotentials to projector augmented-wave method, Phys Rev B 1999, 59(3), 1758-1775.
27. Blöchl, P. E. Projected augmented-wave method. Phys Rev B 1994, 50(24), 17953-17979.
28. Heyd, J.; Peralta, J. E.; Scuseria, G. E.; Martin, R. L. Energy band gaps and lattice parameters evaluated with the Heyd-Scuseria-Ernzerhof screened hydrid functional. J. Chem. Phys 2005, 123(17), 174101-1.
29. Li, Y.; Raghavan, R.; Wagner, N. A.; Davidowski, S. K.; Baggetto, L.; Zhao, R.; Cheng, Q.; Yarger, J. L.; Veith, G. M.; Ellis-Terrell, C.; Miller, M. A.; Chan, K. S.; Chan, C. K. Type I clathrates as novel silicon anodes: an electrochemical and structural investigation. Advanced Science 2015, 2(6), 1500057.
30. Chan, K. S.; Miller, M. A.; Ellis-Terrell, C.; Chan, C. K. Synthesis and characterization of empty silicon clathrates for anode applications in Li-ion batteries. MRS Advances 2016, 1(45), 3043-3048, DOI: 10.1557/adv.2016.434.

31. Chan, K. S.; Miller, M. A.; Liang, W.; Ellis-Terrell, C.; Chan, C. K. First principles and experimental studies of empty Si_{46} as anode materials for Li-ion batteries. J. Mater. Res. 2016, 31(23), 3657-3665, DOI: 10.1557/jmr.2016.408.
32. Zhang, Y.; Zhang, X. G.; Zhang, H. L.; Zhao, Z. G., Li, F.; Liu, C.; Cheng, H. M. Composite anode mateiral of silicon/graphite/carbon nanotubes for Li-ion batteries. Electrochimica Acta. 2006, 51, 4994-5000.
33. Yoon, T.; Nguyen, C. C.; Seo, D. M.; Lucht, B. L. Capacity fading mechanisms of silicon nanoparticle negative electrodes for Lithium ion batteries. Journal of The Electrochemical Society. 2015, 162(12) A2325-A2330.
34. Wang, S. Q.; Ye, H. Q. *Ab initio* elastic constants for the lonsdaleite phases of C, Si and Ge. J. Phys.: Condens. Matter 2003, 15(3), 5307-5134.
35. He, J.; Guo, L.; Guo, X.; Liu, R.; Tian, Y.; Wang,H.; Gao, C. Predicting hardness of dense C_3N_4 polymorphs. Appl. Phys. Lett. 2006, 88(10), 101906-1 – 101906-3.
36. Teter, D. M. Computational alchemy: the search for new superhard materials. MRS Bull. 1998, 23(1), 22-27, DOI: 10.1557/S0883769400031420.
37. He, H.; Sekine, T.; Kobayashi, T.; Hirosaki, H.; Suzuki, I. Shock-induced phase transition of β−Si_3N_4 to c−Si_3N_4. Phys. Rev. B 2000, 62(17), 11412-11417.
38. Jiang, J. Z.; Lindelov, H.; Gerward, L.; Ståhl, K.; Recio, J. M.; Mori-Sanchez, P.; Carlson, S.; Mezouar, M.; Dooryhee, E.; Fitch, A.; Frost, D. J. Compressibility and thermal expansion of cubic silicon nitride. Phys. Rev. B 2002, 65(16), 161202-1 – 16120-4.
39. Carnahan, R. D. Elastic properties of silicon carbide. J. Am. Ceram. Soc. 1968, 51(4), 223-224.
40. Guloy, A. M.; Ramlau, R.; Tang, Z.; Schnelle, W.; Baitinger, M.; Grin, Y. A guest-free germanium clathrate. Nature 2006, 443, 320-323, DOI: 10.1038/nature05145.